JAAS

Accepted Manuscript

This is an *Accepted Manuscript*, which has been through the Royal Society of Chemistry peer review process and has been accepted for publication.

Accepted Manuscripts are published online shortly after acceptance, before technical editing, formatting and proof reading. Using this free service, authors can make their results available to the community, in citable form, before we publish the edited article. We will replace this *Accepted Manuscript* with the edited and formatted *Advance Article* as soon as it is available.

You can find more information about *Accepted Manuscripts* in the Information for Authors.

Please note that technical editing may introduce minor changes to the text and/or graphics, which may alter content. The journal's standard Terms & Conditions and the Ethical guidelines still apply. In no event shall the Royal Society of Chemistry be held responsible for any errors or omissions in this *Accepted Manuscript* or any consequences arising from the use of any information it contains.

ROYAL SOCIETY OF CHEMISTRY

www.rsc.org/jaas

Journal Name Journal of Analytical Atomic Spectrometry Dynamic Article Links ►

Cite this: DOI: 10.1039/c0xx00000x

www.rsc.org/xxxxxx

ARTICLE TYPE

Double-Pulse LIBS Combining Short and Long Nanosecond Pulses in the Microjoule Range

Islam Y. Elnasharty,[a] François R. Doucet,[b*] Jean-Francois Y. Gravel ,[b†] Paul Bouchard,[b] and Mohamad Sabsabi[b]

Received (in XXX, XXX) Xth XXXXXXXXX 20XX, Accepted Xth XXXXXXXXX 20XX
DOI: 10.1039/b000000x

[a] *National Institute of Laser Enhanced Science (NILES), Cairo University, Giza, Egypt.*
[b] *National Research Council of Canada (NRC), Energy, Mining and Environment Portfolio,75 de Mortagne Blvd., Boucherville, Québec, Canada,*
[†] *Formerly with NRC, now with: INO, 2740 Einstein Street, Québec (Québec), Canada, G1P 4S4*
E-mail: francois.doucet@cnrc-nrc.gc.ca

*Author to whom correspondence should be sent

The present study investigates the collinear double-pulse LIBS (DP-LIBS) configuration using microjoule nanosecond pulses. It is shown that this approach can achieve typical double pulse improvement in the analytical performances for elemental analysis of aluminium alloys. In addition, the effect of the chronological sequence of the short and long nanosecond pulses in collinear DP-LIBS experiment was also studied. The results show a significant increase of the intensity and repeatability of the emission signals in the double pulse configuration. Standard DP-LIBS signal improvement over signal-to-noise ratio and signal-to-background ratio for the analytical lines of different elements has been observed in comparison to single pulse LIBS of equal energy. Limits of detection in the low µg g^{-1} range have been obtained for the different elements studied. The improvement resulting from the use of DP-LIBS was about 2-4 fold when compared to SP-LIBS in all cases. These results are useful in the context of studies investigating how the µLIBS will assist in the development of portable LIBS systems and improve the utility of this spectroscopy technique for field applications. Finally, the plasma temperature is found to be approximately less than 10% higher with the double-pulse.

A. Introduction

Over the recent years, the laser-induced breakdown spectroscopy (LIBS) technique has drawn much attention because of many key advantages: (i) no sample preparation is required, (ii) stand-off and *in situ* real-time analysis, (iii) multi-element measurements on different samples (solids, liquids and gases), (iv) non contact nature, and (v) minimally invasive analysis since only a few micrograms of the sample is usually required for the analysis. However, the is often inferred from the literature that LIBS performance in terms of detection limits achievable are in the µg g^{-1} range.[1-3] On the other hand, LIBS demonstrates incomparable absolute detection limit. In fact, low ppm (w/w) as relative detection limit for a few nanograms of ablated sample means that femtograms of matter can be detected.

With the aim to improve the sensitivity and the repeatability of the LIBS, several approaches have been proposed. These approaches include studying the influence of various experimental parameters on the laser ablation process as well as understanding how these parameters might affect the overall analytical signals. For instance, the interaction of the laser induced plasma (LIP) with electric or magnetic fields, [4-6] the formation of the plasma in a modified atmosphere [7], the effect of the laser wavelength on the laser-induced plasma [8], the use of ultra- short (tens of *fs*) [9, 10] or long (hundreds of *ns*) laser pulses [11] and the influence of laser irradiance on plasma parameters [12] have been reported.

One avenue that can be followed to enhance the intensity and repeatability of the laser-induced plasma emission consists in using two successive laser pulses instead of only one as in conventional LIBS. In the so-called "double-pulse LIBS" (DP-LIBS) approach, the two laser pulses are temporally separated by a few to hundreds of microseconds and the plasma emission signal is recorded at a certain delay time following the second pulse. The vast majority of DP-LIBS studies use either collinear or orthogonal propagation geometries. In the collinear configuration, both laser pulses have the same axis of propagation and are directed normal to the sample surface. The first pulse induces plasma formation and is followed by the second pulse that may ablate additional material but contributes mainly to further excitation of the plasma through reheating. This

configuration is popular because it is the most practical beam arrangement for remote, on-site, and online analysis. In the orthogonal double pulse configuration, there are two different modes referred to reheating and pre-ablation spark. In reheating mode, the first pulse irradiates the sample at normal incidence and is used in the ablation step (i.e. producing LIP), while the second pulse propagates parallel to the sample surface just above the ablation spot and is used to reheat the generated plasma. In pre-ablation spark mode, the first pulse is focused parallel to and some distance above the sample surface and is used for producing a weak plasma in air just above the analysis point. As a consequence, the first pulse creates a weakly ionized, rarefied atmosphere which locally reduces the ambient pressure over the sample surface. This atmospheric effect enhances the plasma ionization and increases the ablated mass upon the target with the second pulse (orthogonal with the first pulse). From a practical point of view, the orthogonal arrangement introduces certain constraints since it is using a complicated experimental setup based on a non-straightforward alignment between the generated tiny plasma and the reheating or pre-ablation beam. [13-15] Nevertheless, several combinations of the DP-LIBS approach have been studied such as: (i) using the same pulse duration and wavelength for both pulses, [16,17] (ii) using different pulse durations but the same wavelength, [18,19] (iii) using different wavelengths but the same pulse duration, [20,21] and (iv) using a combination of laser beams. [22-24]

According to recent studies, the DP-LIBS approach shows a significant improvement in the analytical performance, typically over an order of magnitude, along with lower LODs. [19,21] Several possible mechanisms have been proposed in order to explain the emission signal enhancement, such as (i) Sample heating effect (interaction of the second pulse with the modified surface where the first pulse heats the sample), (ii) Pulse-plasma coupling effect (interaction of the second pulse with the early stages of the plasma ignited by the first pulse), (iii) atmospheric effects (ambient gas rarefaction). [25]

To the best of our knowledge, most of the DP-LIBS applications in the nanosecond regime utilize laser pulse energies in the range of a few to hundreds of mJ and the typical laser focal spot sizes are on the order of hundreds of microns. In order to reach such a range of pulse energies, large (i.e. laboratory-type) laser systems must be used, which are not suitable for portable LIBS systems for on-site measurements. More recently, studies have shown that laser pulse energies in the hundreds of microjoules range could be used to create LIBS plasmas while still achieving sensitivities comparable to the conventional LIBS technique. This regime of operation is termed as μLIBS.[13,15] Pulse energies on the order of a hundred of microjoules can be obtained from compact fiber lasers or microchip lasers. [26,27]. Understanding the regime of DP mode operating in the micro joule range will be useful in the context of studies investigating how the μLIBS will assist in the development of portable LIBS systems and improve the utility of this spectroscopy technique for field applications. The present work reports the first results from LIBS analysis in double-pulse mode using laser pulse energies in the microjoule range. The case of laser-induced plasmas formed from aluminum alloys in atmospheric air was studied. Two IR laser beams in collinear configuration have been combined for the double pulse experiments. The first beam was emitted from a compact fiber laser with a long pulse duration of 200 ns and was used for ablation. The second beam was produced by a Nd:YAG flash lamp-pump laser with a short pulse duration of 5 ns and was used for re-excitation of the generated plasma. The pulse energy for each case was set to 250 μJ for double pulse experiment; on the other hand, for the single pulse approach, the total energy was set to 500 μJ (i.e. 250 + 250 μJ). Spectral emission intensity enhancement, signal-to-noise (SNR) and signal-to-background (SBR) ratios as well as LIBS analytical performances were monitored throughout the experiments. The influence of the interpulse delay and of the laser pulses chronological sequence was also investigated. Finally, in order to provide better understanding about the origin of the observed LIBS signal improvement, temporal evolution of the plasma temperature was also measured for both single- and double-pulse experiments.

B. Experimental setup

A schematic diagram of the experimental arrangement used in this work is presented in Fig. 1. The setup is composed of two laser sources, the first is a high power pulsed fiber laser model G3 SP-20P-HS series (SPI Lasers, Southampton, UK) delivering high peak power up to 11 kW with 20 W average output power. The laser operated at its fundamental wavelength (λ = 1064 nm) with an emission band width $\Delta\lambda$ (FWHM) < 10 nm. Furthermore, it may be operated at 15 Hz with different energy outputs (i.e. 40 μJ up to 800 μJ per pulse) and the pulse width can be tuned from 10 ns up to 200 ns (FWHM), depending on the repetition rate and the seeding waveform selected leading to average power between 0.6 to 12 mW. The laser energy output was set by feeding a control voltage to the laser amplifier and monitored using a low power thermal head sensor (30A-5H-V1-ROHS, Ophir Optronics Ltd.) connected to a laser power meter (Nova II, Ophir Optronics Ltd). The pulse width (FWHM) was set to 200 ns. The output of the fiber laser was coupled to the Beam Expander Telescope (BET) model PT-P00399 (SPI Lasers) with magnification of 8.7X. The laser beam was sent through a UV fused silica broadband beamsplitter (BS, POLKA-DOT 70/30, Edmund Optics) that provides a split ratio of 70:30 (R:T), which is nearly constant over the 250 nm – 2.0 μm spectral range.

The secondary excitation source is a Q-switched Nd:YAG laser (Minilite^{TM} ML II, Continuum). The wavelength was 1064 nm and the repetition rate was 15 Hz, with a fixed pulse width of 5 ns (FWHM). The laser energy was generally set at 250 μJ during the double-pulse experiments (after the beam splitter). It was measured with a low energy pyroelectric head detector (PE10-SH-v2, Ophir Optronics Ltd.) connected to a laser power/energy display (Nova II, Ophir Optronics Ltd). The laser beam first goes through a 5X BET; it is then reflected twice (first, by a high-reflectivity mirror and second, by the beam splitter) before hitting the target surface at normal incidence. The beam expender was added to adjust the size of the Nd:YAG laser to match the size of the fiber laser (i.e. 8 mm). In addition, the purpose of the beam expender is to allow smaller beam waist to reach higher fluence on the target.

Both laser beams were combined and aligned in a collinear arrangement by passing through the beam splitter. Subsequently, they were focused onto the sample surface at normal incidence by means of a plano-convex lens (PLCX-25.4-38.6-C-1064 CVI Melles Griot, New Mexico, USA) of 75 mm focal length. This combination of optics, for each laser source, results in a focal spot of ≈ 30 μm in diameter and leads to a fluence of ≈ 35 Jcm^{-2}. Additionally, the beam waist was set at the sample surface considering the limited Rayleigh range of 800 μm. The two lasers were temporally synchronized using a programmable trigger delay/pulse generator (Stanford Research System, Inc., Model DG535) so that the laser pulses arrive after a selected time delay. The delay between laser pulses was varied from Δt = 0 (two simultaneous pulses) up to Δt = 2 μs.

Light emitted from the plasma plume was imaged by using a corrected triplet lens (diam. = 25.4 mm, f = 45 mm, Edmund

Optics, New Jersey, USA), located at 70 mm from the target and at 18° off the normal to the target surface, onto the optical fiber bundle (length: 10 m, bundle: 25 × 120 µm-diameter fibres, bundle active area diameter: 0.7 mm, configuration: round (input) to line (output)), placed at ~13 cm behind the collecting lens. The position and the angle of the optical fiber were determined by the optimization of the signal in order to include all the plasma emission, so that the integrated emission from all the regions of the plasma could be acquired.

For light dispersion and detection, a Czerny-Turner spectrometer (VM 504, Acton Research Co) was used. Its focal length was 0.39 m while its effective aperture was *f* / 5.4. The spectrometer was equipped with a grating of 1200 lines/mm blazed at 150 nm. The corresponding linear dispersion was ≈ 1.3nm/mm. The spectrometer was coupled to an intensified charge-coupled device (ICCD) detector (iStar DH-734-25F-03, Andor Technology) containing 1024×1024 pixels of dimensions 19.5 µm^2. The optic fiber was used as the entrance slit of the spectrometer, which provides a 120 µm wide × 3 mm height slit at the spectrometer entrance. The spectral width of the intensified acquisition window was ≈ 26 nm while the spectral resolution for this system was ≈ 0.156 nm. In terms of spectral emission acquisition in the double pulse configuration, the gate detection delay t_d was set to 500 ns relatively to the second pulse. Detection gate width t_g was set to 10 µs.

The parametric study (i.e. spectral enhancement, SNR, SBR and interpulse delay investigations) was performed using a certified aluminum alloy manufactured by Alcan Inc. (standard 1200 AG) that contains 0.016% of Mg, 0.025% of Mn and 0.17% of Si while the standard (3003 AG) that contains < 0.7 % of Fe was used for plasma temperature characterizations. Additionally, for LIBS analytical measurements, up to seven certified aluminum alloy standards were used, with concentration of Mg ranging from 0.0041% to 1.13%, and those of Mn from 0.025% to 1.1% while those of Si ranging from 0.17% to 9.17%. The emission lines that were considered during all experiments were Mg (I) 285.2 nm, Mn (I) 279.46 nm and Si (I) 288.16 nm. It is important to note that the Mn I 279.552 was chosen because of its presence in the window, there is a possibility of a spectral interference with Mg II at 279.552 nm. A better choice for Mn would have been 403.45 nm.

Three motorized stages model UTM-100CC1HL (Newport, Irvine, CA, USA), controlled by a universal motion controller model ESP300 (Newport) were used to move the sample from site to site. Data acquisition was realized using a computer code developed in LabVIEW 7.1 (National Instruments, Austin, TX, USA) which synchronized the acquisition with the samples' translation in a manner to refresh the surface between each laser shot.

In order to increase the repeatability, the measurements were done at 250 different spots seperated by a few millimeters to take into account any lack of sample homogeneity. These 250 spectra were accumulated in a single acquisition file. For each experiment, 3 files were taken and the statistics were done by taking the average of the 250 spectra for each file; the mean and the associated standard deviation were then calculated over those 3 files.

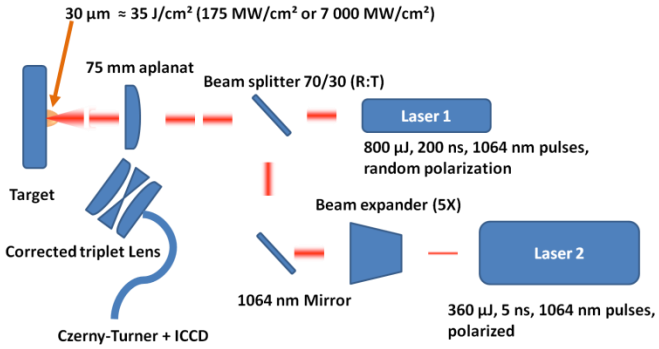

Fig. 1. Schematic diagram of the experimental setup used for the double-pulse LIBS arrangement.

C. Results and discussions

The LIBS spectra obtained from the aluminium alloy sample (1200 AG) for single- and double-pulse configurations under the optimized temporal conditions (i.e. interpulse interval Δt = 1µs, detection delay t_d = 500 ns and the gate width t_g = 10 µs) are presented in Fig. 2 (a). For the DP-LIBS and single pulse measurements, the pulse energy was fixed at 250 µJ for each pulse. The laser sequence combination between two pulses was set with the long pulse duration (i.e. 200 ns) first, followed by the short one (i.e. 5 ns). On the other hand, the SP measurements were carried out with 250 µJ either for 200 ns and 5 ns pulse durations. As can be seen from Fig. 2 (a) the DP-LIBS spectrum shows a very clear enhancement of emission intensity for all lines compared to the spectra obtained with SP of equal energy for the used pulse durations. The observed enhancement is more than 5 fold.

Interestingly, Fig. 2 (a) further reveals an important feature: the LIBS signal intensity obtained from the SP measurement is more intense with the 200 ns pulse than with the 5 ns pulse. It has been recently reported[27] that the combined used of a high quality beam (M2 < 1.8) and of a long nanosecond pulse regime is responsible for the decrease of the plasma shielding effect during the ablation phase, thus leading to a higher level of ablated mass yield.Therefore, the enhancement "long vs short pulse" could be attributed to the higher ablated mass resulting from the use of a long nanosecond laser pulse, which in turn leads to a higher number of emitting atoms in the plasma.[27]

Comparison between the DP-LIBS spectrum and the arithmetic summation of SP-LIBS spectrum of different pulse durations (i.e. 200 ns only + 5 ns only) is showed in Fig. 2 (b), an enhancement of more than 4 fold is also observed for all lines.

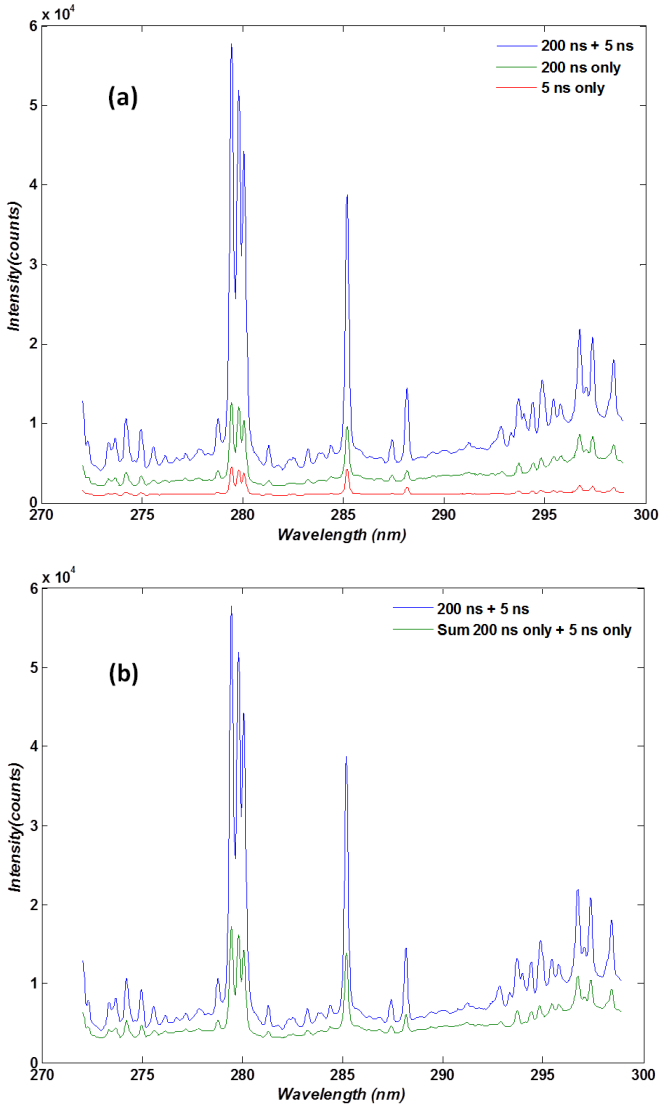

Fig. 2. Comparison of the LIBS spectral intensities from the aluminum alloy sample (1200 AG) (a) corresponding to the double pulse (blue trace) and single pulses of different pulse durations (5ns red trace and 200 ns green trace). A total energy of 500 µJ (i.e. 250 + 250 µJ) and a combination of 200 ns and 5 ns pulse durations with an interpulse delay Δt of 1µs were used in the double pulse experiment. A pulse energy of 250 µJ with duration of 200 ns or 5 ns only (red and green traces) was employed in the acquisition of the single pulses spectra. The detection delay t_d and the gate width t_g were fixed at 500 ns and 10 µs, respectively, for all experiments; (b) corresponding to the double pulse (blue trace) and arithmetic summation of single pulses of different pulse durations (i.e. 200 ns only + 5 ns only) (green trace) acquisitions.

C.1. Influence of the interpulse interval Δt on emission intensities

The influence of the interpulse delay on signal-to-noise ratio (SN) and the signal-to-background (SB) has been studied to determine the ideal interpulse delay. The SN was calculated using the ratio of the net peak height divided by the root-mean-square noise of this signal which is equivalent to SN = [RSD]$^{-1}$.[35] On the other hand, the SB was calculated using the ratio of the net peak height over the average value of the continuum over 25 pixels. The LIBS emission signals in terms of SN and SB for the different neutral lines (Mg (I) 285.2 nm, Mn (I) 279.46 nm and Si (I) 288.16 nm) are presented in Fig 3. The delay between the two laser pulses Δt plays a key role in the double-pulse experiment. Fig. 3 (a) and (b) shows respectively the double-pulse SNR and SBR as a function of the interpulse delay Δt. The interpulse delay ranges from Δt = 0 to 2 µs with fixed detection delay t_d at 500 ns and gate width t_g at 10 µs. It is important to note that the data points at Δt = 0 are equivalent to a single pulse measurement. In other words, at Δt = 0, the two pulses are fired simultaneously and are overlapped in time; therefore, two pulses of equal energy (i.e. $E_1 = E_2$ = 250 µJ) fired at the same time will be considered in this paper as equivalent to a single pulse measurement with pulse energy equal to E_1+E_2 = 500 µJ. According to Fig. 3 (a) and (b), the signal intensity increases significantly with increasing separation of the pulses compared to the single pulse scheme (Δt = 0) and the maximum SNR and SBR values are reached at an interpulse delay value of 1 µs for all neutral lines studied. Thereafter, the intensity starts to decrease. The continuous increasing of emission in the first regime (i.e. from Δt = 0 to Δt = 1µs) can be attributed to a steady interaction of the second pulse with the plasma plume expanding away from the target (i.e. reheating of the plasma and improved ablated mass)). On the other hand, the decrease of the signal intensity for the longer interpulse interval values (i.e. Δt > 1µs) could be related to a decrease of the plasma density due to the expansion of the preplasma at longer interpluse delays. Furthermore, at longer interpulse intervals, the preplasma electron density decreases significantly, thus lowering the coupling efficiency of the second pulse.[28,29] In addition, the enhancement factor for the 3 neutral lines has been calculated using the ratio of the double pulse over the single pulse LIBS line intensity at the same total energy (i.e. double pulse: E_1+E_2 over 2 single pulses with Δt = 0). From Fig. 3 (a) and (b), for both SNR and SBR, the enhancement factor for the LIBS signal in double-pulse configuration at an interpulse delay of 1µs is more than 3 fold compared to the single-pulse case.

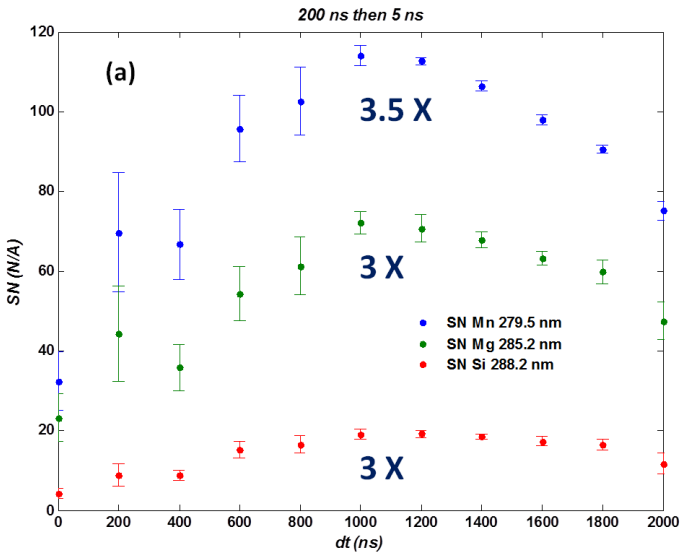

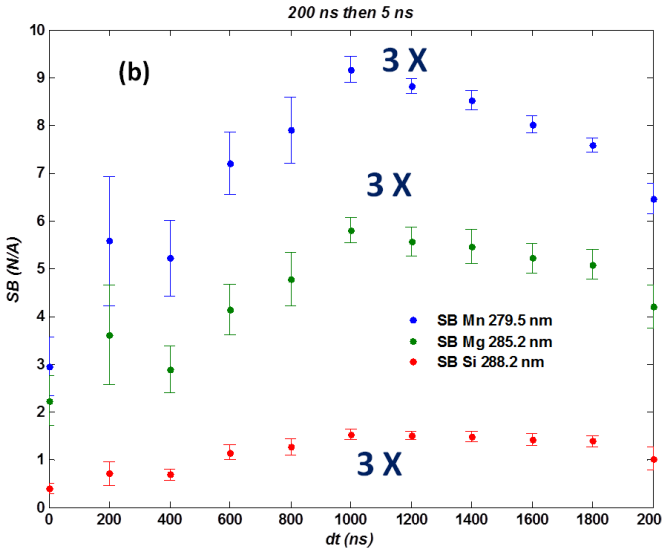

Fig. 3 (a) Signal-to-Noise ratio SN and (b) Signal-to-Background ratio SB as a function of the interpulse delay Δt, with detection delay t_d = 500 ns and gate width t_g = 10 µs. EF is the enhancement factor calculated for each spectral line.

On the basis of the recent work reporting an enhancement of the ablated mass yield with long nanosecond pulses in comparison to short nanosecond pulses[27], it is surmised that the chronological sequence (rank combination) of the two different pulse durations could affect the emission properties of the DP-LIBS plasma, including the spectral line and background intensities. Therefore, the two possible rank combinations were studied and the results are presented in Table 1. The table shows the SNR and SBR values of different neutral emission lines for different pulse duration and rank combination sequences (i.e. a 200 ns followed by a 5 ns or v). The interpulse delay Δt was set to the optimal value for both rank combinations (1 µs) and the detection delay t_d and the gate width t_g were fixed at 500 ns and 10 µs, respectively. Surprisingly, for all elements, the results obtained, in table 2, show that the different rank combination / pulse duration sequences have no significant impact on the SNR and SBR values. This point indicates that the nanosecond DP-LIBS scheme shows no dependency on the combination rank over laser pulses duration. The results presented in table 1 and 2 are suggesting that the second pulse is ablating new material in the plasma as well as reheating the plasma.

Table 1 SNR and SBR values for neutral emission lines with different sequences of pulse duration / rank combination. The interpulse delay Δt was set to 1 µs and the detection delay t_d and the gate width t_g were fixed at 500 ns and 10 µs, respectively.

Combination sequence	Element/line	SNR	SBR
200 ns then 5 ns	Mn (I) 279.46 nm	114	9.2
5 ns then 200 ns		114	9.2
200 ns then 5 ns	Mg (I) 285.21 nm	71.0	5.7
5 ns then 200 ns		61.3	4.8
200 ns then 5 ns	Si (I) 288.16 nm	18.8	1.5
5 ns then 200 ns		25.2	2.0

C.2. Excitation temperature measurements

The plasma temperature has been calculated for the purpose of characterizing and finding the differences between the plasmas generated in the single- and the double-pulse (DP: 5 ns than 200 ns) arrangements and are presented in table 2. Using the Boltzmann plot method described in ref. 30, with the assumption of local thermodynamic equilibrium and optical thinness of the plasma, the excitation temperature of the produced plasma was determined. Table 2 shows the comparison between plasma temperatures for single- and double-pulse modes at 3 different delay times (0.2, 1 and 1.5 µs). The delay times in table 2 allow observation of the temporal evolution of the plasma temperature. As can been seen, the temporal evolution of the temperatures for the two schemes is similar, although the double-pulse mode plasma appears to be slightly hotter (approximately 15%) which is comparable to the value reported by reference 31. The intensity enhancement observed in the double-pulse mode is probably due to this slight increase of temperature. Additionally, the higher ablated mass related to the use of a long nanosecond pulse increases the number of atoms in the plasma and may also contribute to the global enhancement. In other words, the signal enhancement may be related either to an improvement in the excitation efficiency or to an increase in the number of atoms in the plasma. Those conditions may be found in a hotter plasma or by introducing a larger number of analyte atoms in the gas phase through increasing ablation of the target. [31]

Table 2 Plasma temperatures measured at different delay times (t_d) for single- and double-pulse modes under optimized conditions.

Analytical scheme	Acquisition delay (t_d)	Plasma temperature (K)
SP-LIBS	0.2 µs	7800
DP-LIBS		8500
SP-LIBS	1 µs	6000
DP-LIBS		7000

SP-LIBS	1.5 µs	5500
DP-LIBS		6000

C.3. Analytical figures of merit

In this section, the analytical performances for both single- and double-pulse schemes have been characterized for the trace elements Mn, Mg and Si contained in a certified aluminium alloy sample; the results are reported in Table 3 below. The previously selected optimal conditions (i.e. Δt =1µs, t_d = 500 ns and t_g = 10 µs) have been used for this assessment. It is possible to observe in Table 3 that the linearity is better than 0.97. It appears that manganese linearity is the worst of the emission lines studied; the potential spectral interference of the Mg II line at 279.552 nm is probably responsive for this deterioration. The limit of detection (LOD) was calculated according to the IUPAC definition (3σ convention):

$$LOD = 3 \times \sigma_{bl} \times S$$

where σ_{bl} is a measure of the standard deviation on the blank sample and S is the sensitivity of the calibration curve.[32] As can be seen in Table 3, the LOD calculations show an improvement of about 2-3 fold for all elements using DP-LIBS over SP-LIBS.

The above LODs measured in the DP-LIBS configuration are comparable to those reported in the literature for pulse energy levels up to three orders of magnitude higher.[1-3] The main cause could be attributed to an increase of the mass ablated with the second pulse. Various studies have been conducted to support this evidence. For instance, a theoretical model published by Rai *et. al.* [33] indicates that, in the collinear configuration, the second laser pulse increases the ablated mass by more than 3.5 times in comparison with the single pulse mode. Furthermore, Cristoforetti *et. al.* [34] investigated the effect of laser parameters (pulse durations and pulse energies) on the line intensities, atomized ablated mass and crater volume for both single- and double pulse configurations. They conclude from this investigation that the plasma shielding process with nanosecond pulse is a complex phenomenon. In the present study, the strong ablation behavior of the long nanosecond pulse regime provided by the fiber laser (7.7 µm/pulse, see ref. 27), combined to high peak irradiance levels for plasma shielding (0.17 or 7 GW cm^{-2} for pulse durations of 200 ns or 5 ns, respectively), could explain the observed DP enhancement.

Table 3 Limits of detection (LOD) and enhancement factors calculated for the single- and double-pulse configurations under optimized conditions.

Analytical scheme	Element	R^2	Detection limit (µg g^{-1})	Enhancement
SP-LIBS	Mn (I) 279.46 nm	0.97	8	≈ 2.5
DP-LIBS		0.98	3	
SP-LIBS	Mg (I) 285.21 nm	.995	2	≈ 3
DP-LIBS		.993	0.6	
SP-LIBS	Si (I) 288.16 nm	0.998	90	≈ 2
DP-LIBS		0.999	40	

Conclusion

This paper reports the first demonstration that the signal enhancement effect associated with the double-pulse regime in LIBS can occur with low (microjoule) pulse energy levels. SN and SB improvements of more than 3 fold, in comparison with the single -pulse case, have been found for different neutral lines. The optimum interpulse delay is found to be 1 µs. Additionally, the comparison between the plasma temperatures obtained in single- and double-pulse arrangements reveals that the latter yields slightly hotter plasmas. Moreover, improvements in the analytical figure of merit, such as the LOD for double-pulse LIBS, weres 2-3 fold in comparison to the single-pulse case. It is difficult to conclude that the use of a long nanosecond pulse regime, which is known to ablate more material, is solely responsible for the double- pulse enhancement. This is due, in part, to the difficulty of identifying the exact contribution of each of the two different phenomena (additional ablation and plasma reheating). This enhancement in emission intensities could be explained by the presence of a larger ablated mass, resulting from the use of long nanosecond pulses, as well as an increase of the population densities of the upper levels of the spectral lines, due to the higher plasma temperature. Further experiments would be required in order to isolate the ablation and plasma reheating contributions in the double pulse experiments using, for instance, different pulse energies. Finally, these results are useful in the context of studies investigating how the µLIBS will assist in the development of portable LIBS systems and improve the utility of this spectroscopy technique for field applications.

Acknowledgements

The authors would like to thank the National Research Council of Canada for the followship, and Mr. Francis Boismenu of the EME-NRC team for experimental setup assistance.

References

1 R. Noll, *Laser-Induced Breakdown Spectroscopy*: Fundamentals and Applications, Springer, Berlin, 2012.
2 D. W. Hahn, N. Omenetto, *Appl. Spectrosc.*, 2012, **66**, 347-419.

3 F. J. Fortes, J. Moros, P. Lucena, L. M. Cabalin, J. J. Laserna, *Anal. Chem.*, 2013, **85** (2), 640-669

4 K. A. Tereszchuk, J. M. Vadillo and J. J. Laserna, *Appl. Spectrosc.*, 2008, **62**, 1262 (ajoute page).

5 X. K. Shen, Y. F. Lu, T. Gebre, H. Ling and Y. X. Han, *J. Appl. Phys.*, 2006, **100**, 053303.

6 Y. Liu, M. Baudelet and M. Richardson, *J. Anal. At. Spectrom.*, 2010, **25**, 1316–1323.

7 J. S. Cowpe, R. D. Pilkington, J. S. Astin, A. E. Hill, *J. Phys. D: Appl. Phys.* 2009, **42**, 165202-1‑165202-8.

8 Q. Ma, V. Motto-Ros, F. Laye, J. Yu, W. Lei, X. Bai, L. Zheng, H. Zeng, *J. Appl. Phys.* 2012, **111**, 053301-1‑053301-11.

9 E. Axente, S. Noel, J. Hermann, M. Sentis, I. N. Mihailescu, *Appl. Surf. Sci.* 2009, **255**, 9734‑9737.

10 K. F. Al-Shboul, S. S. Harilal, A. Hassanein, *Appl. Phys. Lett.* 2012, **100**, 221106-1‑221106-4.

11 Y. Zhou, S. Tao, B. Wu, *Appl. Phys. Lett.*, 2011, **99**, 051106-1–051106-3.

12 W. F. Luo, X. X. Zhao, Q. B. Sun, C. X. Gao, J. Tang, H. J. Wang, W. Zhao, *Pramana-J. Phys.*, 2010, **74**, 945–959.

13 J. Pender, B. Pearman, J. Scaffidi, S. R. Goode and S. M. Angel, *"Laser-induced breakdown spectroscopy using sequential laser pulses"*, pp. 516-534; P. Fichet, J. L. Lacour, D. Menut, P. Mauchien, A. Rivoallan, *"Micro LIBS technique"*, pp. 539-555; Chapters in *Laser-Induced Breakdown Spectroscopy (LIBS)*: *Fundamentals and Applications*, A. W. Miziolek, V. Palleschi and I. Schechter (Eds.), Cambridge University Press, UK, 2006.

14 D. A. Cremers and L. J. Radziemski, *Handbook of Laser-Induced Breakdown Spectroscopy*, Wiley, New York, USA, 2006.

15 J. Scaffidi, D.A. Cremers and S.M. Angel, *"Dual-Pulse Laser-Induced Breakdown Spectroscopy"*, pp. 137–150; M. T. Taschuk, I. V. Cravetchi, Y. Y. Tsui and R. Fedosejevs, *"Micro-LIBS"*, pp. 173-196; Chapters in *Laser-Induced Breakdown Spectroscopy*, J. P. Singh and S. N. Thakur (Eds.), Elsevier, Amsterdam, 2007.

16 R. Noll, V. Sturm, Ü. Aydin, D. Eilers, C. Gehlen, M. Höhne, A. Lamott, J. Makowe, J. Vrenegor, *Spectrochemi. Acta, Part B*, 2008, **63**, 1159–1166.

17 V. Pinon and D. Anglos, *Spectrochemi. Acta, Part B*, 2009, **64**, 950–960.

18 Y. Maruyama, K. Akaoka, M. Miyabe, I. Wakaida, *Appl. Phys. A*, 2010, **101**, 545‑549.

19 Y. Lu, V. Zorba, X. Mao, R. Zhengb, R. E. Russo, J. *Anal. At. Spectrom.*, 2013, **28**m 743-748.

20 V. Piscitelli, M. A. Martinez, A. J. Fernandez, J. J. Gonzalez, X. L. Mao, R. E. Russo, R. E. *Spectrochim. Acta, Part B*, 2009, **64**, 147-154.

21 K. Rifai, S. Laville, F. Vidal, M. Sabsabi and M. Chaker, *J. Anal. At. Spectrom.*, 2012, **27**, 276.

22 A. Pall, R. D. Waterbury, E. L. Dottery, D. K. Killinger, *Opt. Express*, 2009, **17**, 8857‑8870.

23 M. Weidman, M. Baudelet, S. Palanco. M. Sigman, P. J. Dagdigian, M. Richardson, *Opt. Express*, 2010, **18**, 259‑262.

24 A. Khumaeni, Z. S. Lie, H. Niki, K. Fukumoto, T. Maruyama, K. Kagawa, *Opt. Rev.* 2010, **17**, 285‑289.

25 J. Scaffidi, S. M. Angel, D. A. Cremers, *Anal. Chem.*, 2006, **78**, 25–32.

26 A. Freedman, F. J. Iannarilli Jr., J. C. Wormhoudt, *Spectrochemi. Acta, Part B*, 2005, **60**, 1076-1082.

27 J.F.Y. Gravel, F. R. Doucet, P. Bouchard and M. Sabsabi, *J. Anal. At. Spectrom.*, 2011, **26**, 1354-1361.

28 L. St-Onge, V. Detalle, M. Sabsabi, Spectrochim. Acta Part B, 2002, **57**, 121–135.

29 Gautier, P. Fichet, D. Menut, J-L. Lacour, D. L'Hermite, J. Dubessy, Spectrochim. Acta Part B, 2005, **60**, 792–804.

30 M. Sabsabi and P. Cielo, Appl. Spectrosc., 1995, **49**, 499–507.

31 R. Sattmann, V. Sturm, R. Noll, J, Phys. D, 1995, **28**, 2181.

32 ISO 11843-2, Capability of detection, Genève, Switzerland, 2000.

33 V. N. Rai, F. Y. Yueh, J. P. Singh, *Appl. Optics* 2008, **47**, G30‑G37.

34 G. Cristoforetti, G. Lorenzetti, P. A. Benedetti, E. Tognoni, S. Legnaioli and V. Palleschi, , J. Phys. D: Appl. Phys., 2009, **42**, 225207.

35 J.D. Ingle, S.R. Crouch, *Spectrochemical Analysis*, Prentice Hall, New Jersey, 1988, p.8.